

See discussions, stats, and author profiles for this publication at: <https://www.researchgate.net/publication/21394221>

Fracture prediction for the proximal femur using finite element models: Part I - Linear analysis

Article in *Journal of Biomechanical Engineering* · December 1991

Source: PubMed

CITATIONS

181

3 authors, including:



Jeffrey Lotz

University of California, San Francisco

281 PUBLICATIONS **9,650** CITATIONS

[SEE PROFILE](#)



Wilson C Hayes

Hayes + Associates, Inc.

333 PUBLICATIONS **23,411** CITATIONS

[SEE PROFILE](#)

Some of the authors of this publication are also working on these related projects:



Role of the cartilage endplate in spinal disc degeneration [View project](#)



Phenotypes of pathologic vertebral endplate degeneration [View project](#)

Fracture Prediction for the Proximal Femur Using Finite Element Models: Part I—Linear Analysis

J. C. Lotz¹

E. J. Cheal

W. C. Hayes

Orthopaedic Biomechanics Laboratory,
Department of Orthopaedic Surgery,
Charles A. Dana Research Institute,
Beth Israel Hospital and
Harvard Medical School,
Boston, MA 02215

Over 90 percent of the more than 250,000 hip fractures that occur annually in the United States are the result of falls from standing height. Despite this, the stresses associated with femoral fracture from a fall have not been investigated previously. Our objectives were to use three-dimensional finite element models of the proximal femur (with geometries and material properties based directly on quantitative computed tomography) to compare predicted stress distributions for one-legged stance and for a fall to the lateral greater trochanter. We also wished to test the correspondence between model predictions and in vitro strain gage data and failure loads for cadaveric femora subjected to these loading conditions. An additional goal was to use the model predictions to compare the sensitivity of several imaging sites in the proximal femur which are used for the in vivo prediction of hip fracture risk. In this first of two parts, linear finite element models of two unpaired human cadaveric femora were generated. In Part II, the models were extended to include nonlinear material properties for the cortical and trabecular bone. While there was poor correspondence between strain gage data and model predictions, there was excellent agreement between the in vitro failure data and the linear model, especially using a von Mises effective strain failure criterion. Both the onset of structural yielding (within 22 and 4 percent) and the load at fracture (within 8 and 5 percent) were predicted accurately for the two femora tested. For the simulation of one-legged stance, the peak stresses occurred in the primary compressive trabeculae of the subcapital region. However, for a simulated fall, the peak stresses were in the intertrochanteric region. The Ward's triangle (basiscervical) site commonly used for the clinical assessment of osteoporosis was not heavily loaded in either situation. These findings suggest that the intertrochanteric region may be the most sensitive site for the assessment of fracture risk due to a fall and the subcapital region for fracture risk due to repetitive activities such as walking.

Introduction

Fracture of the hip is a significant problem in the adult population, with more than 250,000 cases reported per year in the United States alone [2]. While evidence suggests that certain therapeutic regimens can retard bone loss and thus stabilize fracture risk [31], these treatments themselves can pose significant health risks. Therefore, it is important to identify and institute therapy for those who are at greatest risk for fracture. Accordingly, many noninvasive techniques have been proposed for the assessment of in vivo hip fracture risk. These methods are typically based on estimates of bone density (by using dual photon absorptiometry or quantitative computed tomography) at various sites within the proximal femur, such as the Ward's triangle region. While generally good correla-

tions between failure loads and bone density have been reported for in vitro studies [44, 32, 9, 18, 29], there has been limited success in using such measures to separate, either retrospectively or prospectively, fracture patients from age- and gender-matched controls [4, 37, 11, 25].

There are several reasons for this difficulty in translating results derived in vitro into more discriminating procedures for assessing fracture risk in vivo. One important reason is that many variables, such as bone strength, loading type (direction and magnitude), and probability of trauma [45, 1, 28] act in concert to determine in vivo fracture risk, whereas when performing in vitro studies, only a few of these parameters are investigated. In addition, in vitro femoral specimens are typically fractured under loading configurations representing one-legged stance. However, spontaneous fractures of the hip during gait, which might be associated with such loading conditions, represents less than 10 percent of all hip fractures [28]. Rather, it appears that most hip fractures are associated with

¹Present address: Failure Analysis Associates, Menlo Park, CA 94025.

Contributed by the Bioengineering Division for publication in the JOURNAL OF BIOMECHANICAL ENGINEERING. Manuscript received by the Bioengineering Division November 5, 1989; revised manuscript received April 15, 1991.

falls, usually from standing height or less. During such falls, the loading conditions are likely much different from those during gait and hence would produce very different stress distributions. Furthermore, the structural significance of "regions of interest" such as Ward's triangle at which noninvasive measurements are made, has not been demonstrated in any rigorous manner, even for simplified loading conditions. Thus, to develop more accurate fracture risk assessments, it is important to understand the structural behavior of the proximal femur from which the location of structurally significant regions may be identified and used for noninvasive assessments of fracture risk.

Toward this end, we have performed a structural analysis of the proximal femur using the finite element method to identify the relative importance of bone geometry, material properties, and loading conditions in the assessment of hip fracture risk. The finite element method presents two main advantages over other techniques for the structural analysis of the proximal femur. The first is that this method allows parametric representation of the complex geometric and material property distributions, which occur in vivo and which normally are difficult to represent with other analytic or experimental techniques. The second advantage is that while an intact bone can be tested to failure only once, a finite element model can be analyzed parametrically to investigate different loading conditions, geometries, and material property distributions.

While application of the finite element method for both two- and three-dimensional analysis of the proximal femur is becoming routine, the majority of published studies investigate issues regarding the use of femoral prostheses, and hence focus on regions distal to the greater trochanter [16, 36, 43]. A few detailed analyses of the femoral neck have been presented, but again, no emphasis was placed on cervical or intertrochanteric fracture [5, 30]. In addition, while finite element analysis has been used with good success to predict the strength of diaphyseal bone [14], similar results have not been presented for structures which are primarily composed of trabecular bone.

For this study, finite element models of intact proximal femora were created using geometry and density data derived noninvasively from quantitative computed tomography images. Quantitative computed tomography was chosen because it has been shown to be an accurate technique for the assessment of intact bone status [10, 34, 13]. In addition, with this imaging modality, both the bone geometry and density can be determined, and consequently it becomes possible to generate finite element models of intact bones with accurate representation of the complex variation of these parameters. The objectives of this investigation were to: 1) use finite element models of intact femora generated by quantitative computed tomography to investigate the isolated structural behavior of the proximal femur subject to loading conditions approximating one-legged stance and one particular type of fall; and 2) test the correspondence between these finite element analyses and in vitro fracture studies of the corresponding intact femora to determine how well this technique can model the complex process of bone failure. Our long term goals are to use the predictions of these models as baseline data to study the structural consequences of bone pathology such as osteoporosis or the presence of metastatic lesions. In this paper we present the results of linear finite element analyses. Nonlinear results are presented in a companion paper [20].

Materials and Methods

Two human femora from two cadavers were used (female, age 66 and 70 years). A separate finite element model was generated for each femur to account for the geometric and material property differences between specimens. Each femur was also loaded to failure, one with simplified one-legged stance and the other with a simulated fall. While it is possible to

analyze multiple loading conditions with a single finite element model, only the single loading condition corresponding to the in vitro mechanical test is presented for each of the two models. After harvesting, the femora were stored at -20°C and subsequently thawed at room temperature just prior to testing. While in a water bath, both bones were imaged using a GE 8800 scanner operating at 120 KVP and 240 MAS. One and one half millimeter thick scans were made perpendicular to the neck axis at 5 mm intervals starting at the base of the femoral neck and extending through the femoral head. Similarly, 1.5 mm thick scans were made perpendicular to the diaphyseal axis at 10 mm intervals beginning at the superior aspect of the lesser trochanter and extending distally for 50 mm. Finally, three, 1.5 mm thick scans were made through the intertrochanteric region at equal angles such that they bisect equally the included angle between the most distal of the neck scans and the most proximal of the diaphyseal scans.

Finite Element Mesh. The computed tomography images were reconstructed off-line using an image processing system (Model FD5000, Gould Inc., San Jose, CA) and in-house software running on a VAX 11/750 (Digital Equipment Corp., Maynard, MA). A finite element mesh, consisting of over 3100 nodes representing 214 cortical and 453 trabecular 20-node isoparametric solid elements (Fig. 1), was generated using the preprocessor FEMGEN (Greatwest Technology Transfer, Minneapolis, MN). The model coordinates were assigned by projecting the computed tomography images on a digitizer (Cybergraph system, Talos Systems, Scottsdale, AZ).

Material Properties. After establishing the mesh geometry, faces of the trabecular elements coincident with each computed tomography slice were superimposed on the appropriate image and the average computed tomography number for each element face was calculated. In addition, computed tomography data for each slice were sampled from each chamber of the phantom included in each scan. A very high positive linear correlation was observed between the computed tomography value versus the percent concentration of K_2HPO_4 for each chamber ($R^2 > 0.99$, $p < 0.001$). The slope and intercept of this line were then used to correct the average data for scanner drift [12]. Next, a computed tomography value for each trabecular element was determined by averaging the data for the two element faces from consecutive images. Using our reported correlations between corrected computed tomography number and directly measured bone modulus and strength [22] these computed tomography data were then converted into estimates of the material properties using the following relations:

$$E = 0.7(\text{QCT})^{1.2} \quad (1)$$

$$S = 0.003(\text{QCT})^{1.4} \quad (2)$$

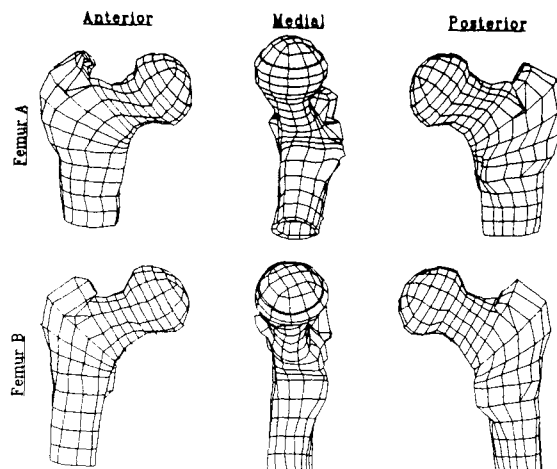


Fig. 1 Meshes for the two finite element models

Table 1 Trabecular bone material properties (all models)

Material Set	% K ₂ HPO ₄ (gm/100 cc)	Density (gm/cc)	Modulus (MPa)	Strength (MPa)
1	4.4	0.22	65	0.60
2	9.1	0.28	160	1.50
3	13.8	0.33	260	2.80
4	18.4	0.39	360	4.10
5	23.1	0.44	480	5.70
6	27.8	0.50	600	7.40
7	32.5	0.56	720	9.20
8	37.1	0.62	840	11.00
9	41.8	0.67	970	13.00
10	46.5	0.73	1100	15.00

Table 2 Cortical material properties—linear models

Model	Location	E ₁	E ₂	E ₃	G ₁₂ GPa	G ₂₃	G ₃₁	ν ₁₂	ν ₁₃	ν ₂₃
A	Diaph	11.0	11.0	16.3	3.46	3.15	3.15	0.58	0.31	0.31
	Meta	7.4	7.4	11.0	2.31	2.11	2.11	0.58	0.31	0.31
	Reduced	2.8	2.8	3.5	0.90	0.82	0.82	0.58	0.31	0.31
B	Diaph	10.5	10.5	15.5	3.28	2.98	2.98	0.58	0.31	0.31
	Meta	7.0	7.0	10.4	2.00	2.20	2.00	0.58	0.31	0.31
	Reduced	3.5	3.5	5.2	1.00	1.10	1.00	0.58	0.31	0.31

where E is the elastic modulus (MPa), S is the compressive strength (MPa) and QCT is the computed tomography equivalent mineral density (gm/100 cc). Due to the large number of trabecular elements, it was impractical to represent the complete range of material properties indicated by the computed tomography data. Instead, 10 different values of material properties were used, each representing a range of bone density of 0.06 gm/cc (Table 1). Each trabecular element was then assigned the material properties of the set which was closest to its estimated value.

The material properties used to represent both the diaphyseal cortical bone and the metaphyseal shell were also based on our direct measurements of bone strength and modulus of the regions [21]. The mesh elements representing the metaphyseal shell were at a minimum 1 mm thick for both models. To reflect a decreased thickness where appropriate (as measured on the contralateral bone of each pair), the elastic modulus was reduced by one third to one half. Consequently, three material sets were used to represent cortical bone within each model: one for diaphyseal bone, a second for the metaphyseal shell, and a third with a reduced elastic modulus for elements less than 1 mm thick (Table 2).

The analyses performed for each bone assumed linear behavior, with the trabecular bone represented as being isotropic and the cortical bone and metaphyseal shell represented as being transversely isotropic. The trabecular bone elastic moduli were highly heterogeneous as determined by computed tomography data, and were assigned a uniform Poisson's ratio of 0.3. The longitudinal and circumferential cortical elastic moduli were determined from our previous studies [21]. The shear moduli, which were not directly measured, were based on the results of Reilly and Burstein [33] and scaled by the particular value of the longitudinal modulus used in each material set (Table 2). For example, Reilly and Burstein presented a value of the shear modulus component G_{12} as 3.60 GPa when the longitudinal modulus E_3 was 17.0 GPa. In this analysis, where the diaphyseal cortical modulus E_3 was 15.5 GPa, the value of the shear modulus component G_{12} was estimated to be $3.60(15.5/17.0)$ or 3.28 GPa.

Applied Loads. Each model was used to analyze a separate load case. The first load case, corresponding to Femur A, consisted of a distributed compressive load (445 N) applied to the superior aspect of the femoral head and directed parallel to the diaphyseal axis (Fig. 2(a)). This load geometry has been shown to approximate one-legged stance [35]. The second load case, corresponding to Femur B, represented one particular type of fall in which the posterolateral aspect of the greater

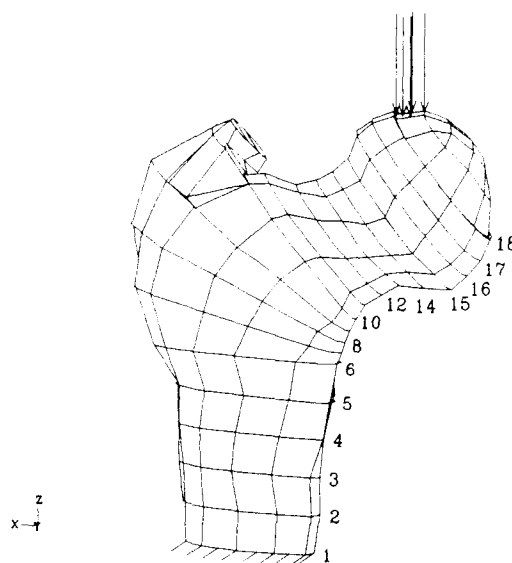


Fig. 2(a) Loads applied to Femur A, simulating one-legged stance. The section numbers are included for reference.

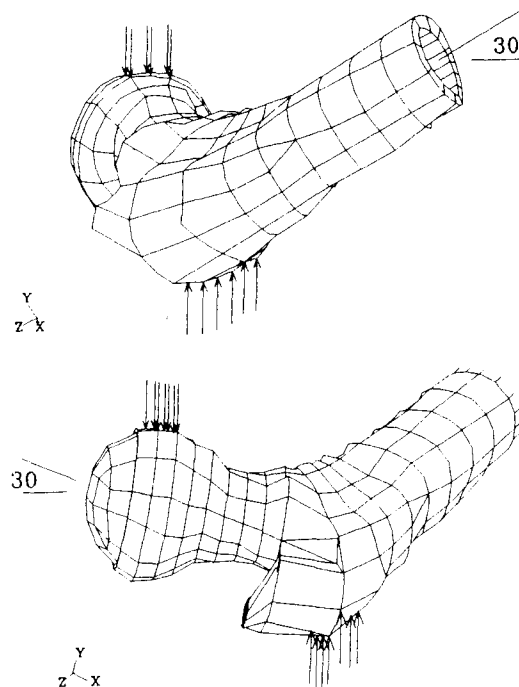


Fig. 2(b) Loads applied to Femur B, simulating a fall. Equal and opposite loads were applied to the femoral head and the greater trochanter.

trochanter comes in contact with the ground [3]. For this case, a posterolaterally directed load (222 N) was applied to the femoral head with an equal and opposite load applied to the lateral greater trochanter (Fig. 2(b)). The direction of the loads were such that both the diaphyseal and cervical axes form an angle of 30 degrees with the plane perpendicular to the applied loads (horizontal). These directions represent the thigh at an angle of 30 degrees to the ground and the torso rotated slightly to the side of contact. For both load cases, the joint load was distributed over 9 adjacent nodes such that the resultant passed through the anatomic center of the femoral head. To balance the applied loads in both models, all nodes on the most distal face of the diaphysis were rigidly constrained. For the fall load case (Femur B) this constrained end condition assumes that during the short time period of impact from an actual fall, the

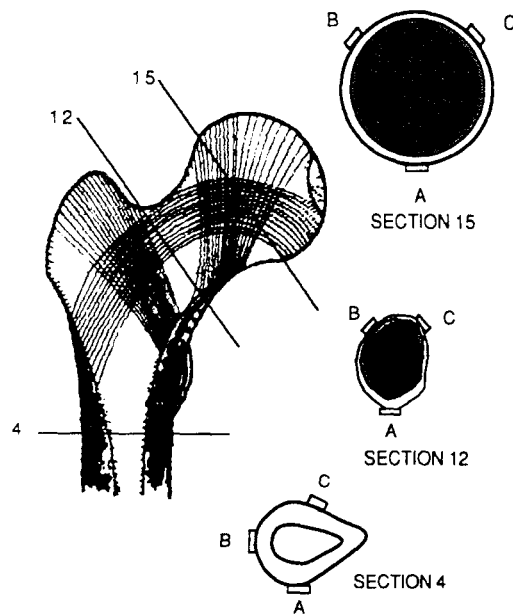


Fig. 3 Strain gage locations for both instrumented femurs. The locations correspond to medial (A), anterior (B), and lateral (C) at section 4, and inferior (A), superior-anterior (B), and superior-posterior (C) at sections 12 and 15.

inertial effects of the lower extremity are dominant and effectively act to constrain the leg against the forces generated at the point of impact.

Failure Criteria. To predict local bone failure a von Mises yield criterion was applied to the stress results for elements representing cortical bone, and both a von Mises and Hoffman yield criterion were applied to the stress results for elements representing trabecular bone. The Hoffman failure theory [15] assumes linear terms to account for different tensile and compressive strengths, and has been demonstrated to fit experimental trabecular bone data well for the $\tau_{xy} - \sigma_{xx}$ plane [41]. Assuming isotropy, the theory is given by

$$C_1 \{\sigma_2 - \sigma_3\}^2 + C_2 \{\sigma_3 - \sigma_1\}^2 + C_3 \{\sigma_1 - \sigma_2\}^2 + C_4 \sigma_1 + C_5 \sigma_2 + C_6 \sigma_3 = 1$$

where

$$C_1 = C_2 = C_3 = \frac{1}{2S_t S_c}$$

$$C_4 = C_5 = C_6 = \frac{1}{S_t} - \frac{1}{S_c}$$

and where σ_i are the principal stresses, S_t is the ultimate strength in tension, and S_c is the ultimate strength in compression. If S_t and S_c are equal, Eq. (3) reduces to the von Mises yield function. These criteria will overestimate the strength under hydrostatic compression since the failure surface is open in the triaxial compression direction of principal stress space. The compressive strength of trabecular bone was estimated directly using our computed tomography-strength regressions (Eq. 2), while the tensile strength was assumed to be approximately one-third the compressive strength [41].

The model results for elements representing the cortical shell, primary compressive trabeculae, and primary tensile trabeculae, are presented separately. The primary compressive trabecular system extends proximally from the superior aspect of the femoral head distally to the medial calcar, while the primary tensile trabecular system traverses along the superior aspect of the femoral neck. By noting the average computed tomography data for element faces coincident with the mesh section locations throughout the femoral neck (Fig. 3), the elements representing either the primary compressive or primary tensile

trabeculae were isolated. At these section locations, the maximum von Mises and/or Hoffman failure stress was calculated for coincident element faces. The maximum effective stress for each element face was then divided by the element tensile strength to determine a critical stress ratio for that element. A peak stress ratio at each section was then determined for each of three element groupings.

Several authors have demonstrated a constant strain at failure for bone, which suggests that a measure of material strain may be a good indicator of bone strength [42]. With this in mind, an effective von Mises strain was also calculated for each element. Based on the results of our trabecular compression tests [22] and literature data for cortical bone [7], a uniform ultimate failure strain of 3 percent was assumed for all materials to calculate the critical strain ratio at failure.

The analyses were performed using ADINA (ADINA Engineering, Inc., Watertown, MA), a general displacement-based finite element code. ADINA provided the interpolation of elemental integration point stresses to the nodal points. In-house software calculated the three-dimensional nodal strains, effective stresses and strains, and principal stresses and their direction cosines.

In Vitro Mechanical Testing. Each femur was sectioned at the mid-diaphysis and the distal end was embedded within an aluminum fixture. Each femur was then instrumented with 9 strain gage rosettes. The location of the gages was such that three rosettes were coplanar at three specified locations: sub-capital, basicervical and subtrochanteric (Fig. 3). The gages used were stacked, 45-degree rosettes with an active gage length of 3.18 mm (#FABR-12-35SX, BLH Electronics, Waltham, MA). The bone surface was prepared and gages bonded using the protocol of Carter et al. [8]. Each gage was then connected as an active branch of a Wheatstone bridge employing one dummy gage (120 ohm) for temperature compensation. Each bridge was part of an Optilog data collection system (Optim Electronics, Gaithersburg, MD) which sequentially sampled each gage. The data were collected from the Optilog using a personal computer (Model AT, IBM Corp., Boca Raton, FL) and commercially available software (Labtech Notebook, Wilmington, MA).

Both femora were then tested to failure using a hydraulic materials testing system (Model 1331, Instron Corp., Canton, MA) in one of the two loading modes corresponding to the finite element analyses. With the distal end rigidly fixed, Femur A was tested to failure with a single load applied to the femoral head and directed parallel to the diaphyseal axis. To simulate a fall, Femur B was positioned such that both the diaphyseal and neck axes formed an angle of 30 degrees with the horizontal. The distal end of the femur was rigidly fixed within a clamp fixture such that the lateral aspect of the greater trochanter was in contact with the platform of the hydraulic actuator. A single vertical load was applied to the femoral head, directed in the anatomic posterolateral direction. Since the distal end of Femur B was rigidly clamped, there existed a possibility that the applied load to the femoral head would exceed the reaction load at the greater trochanter. To determine if this were the case, a second load cell was mounted under the greater trochanter to measure this reaction load. Throughout the testing of Femur B, both the applied load and the reaction load were nearly identical and consequently the assumption of equal and opposite reaction forces were used in the finite element analysis of Femur B.

Results

The load-deflection behavior of the intact bones during the in vitro failure tests is shown in Fig. 4. These plots demonstrate that Femur A began to yield at 1960 N and failed at 3825 N. The resulting fracture was transcervical, passing from the su-

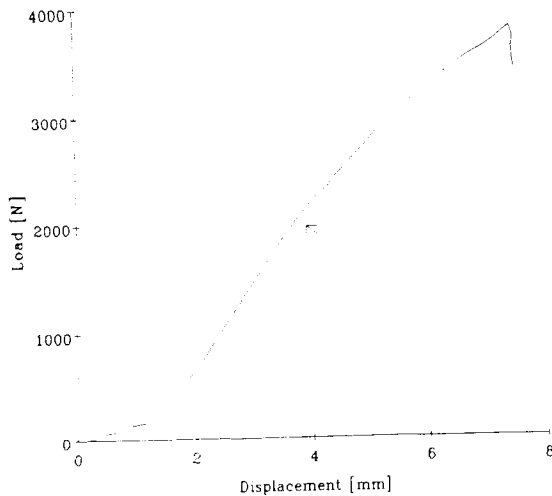


Fig. 4(a) Load-displacement curve for Femur A. The arrow indicates the approximate onset of yielding.

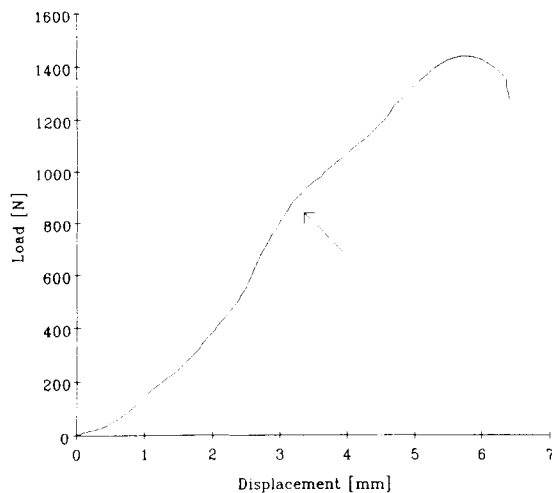


Fig. 4(b) Load-displacement curve for Femur B. The arrow indicates the approximate onset of yielding.

terior aspect of the femoral neck (near section 15) down to the calcar region (near section 10). Femur B began to yield at 770 N and subsequently failed at 1430 N. The resulting fracture in this case was intertrochanteric (between sections 9 and 10). In addition to the recorded load/deflection data, the onset of audible cracking produced by the bones during testing was used to help identify the onset of structural yielding.

Finite Element Analysis. The values of measured and calculated maximum principal strains for each gage location are presented in Tables 3 and 4. The location numbers correspond to model sections (Fig. 2), while the letter designation refers to the circumferential location of the gage within each section (Fig. 3). Strain gage 4B (anterior diaphyseal) of Femur A failed during the in vitro experiment and hence no data were collected at this location. For Femur A, the difference between the model and experimental results varied from between 1 and 200 percent, with the best agreement observed in the diaphyseal region (locations A and C). However, for Femur B, poorer agreement was observed, with the difference between the model and experimental results ranging from 8 to 550 percent. The majority of this variance occurred at six specific gages: 2 for Femur A and 4 for Femur B.

Principal surface stress vectors as predicted by the finite element analyses are presented in Fig. 5. For Femur A, the

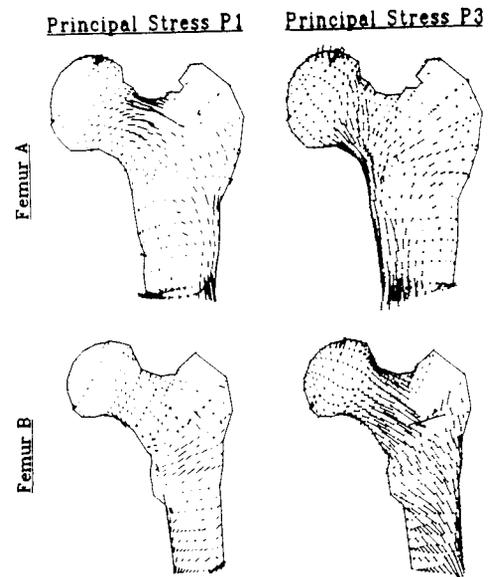


Fig. 5 Principal stress vectors on the posterior surface of Femurs A and B. Cross-bars on the vectors indicate compression.

Table 3 Strain gage/FEA model correspondence—bone A (445 N load)

Location	Principal Strain Results ($\times 10^{-3}$)				Percent Difference	
	FEA		Experiment		P1	P3
4A	0.215	-0.122	0.372	-0.284	-42	-56
4B	0.	0.	0.	0.		
4C	0.211	-0.463	0.769	-0.586	-72	-21
12A	0.817	-0.463	0.286	-0.117	+185	+195
12B	0.925	-0.620	0.414	-0.693	+123	-11
12C	0.171	-0.186	0.168	-0.182	+1	+2
15A	0.327	-0.519	0.489	-0.515	-33	+1
15B	0.832	-0.750	0.563	-0.501	+48	+49
15C	0.282	-0.140	0.563	-0.515	-50	-73

Table 4 Strain gage/FEA model correspondence—bone B (222 N load)

Location	Principal Strain Results ($\times 10^{-3}$)				Percent difference	
	FEA		Experiment		P1	P3
4A	0.607	-0.367	0.227	-0.230	+167	+60
4B	0.422	-0.506	0.176	-0.141	+140	+260
4C	0.568	-0.398	0.363	-0.368	+56	+8
12A	0.548	-0.557	0.119	-0.155	+366	+260
12B	0.676	-0.775	0.749	-1.094	-10	-29
12C	0.430	-0.597	0.331	-0.417	+30	+43
15A	1.165	-1.130	0.237	-0.174	+392	+550
15B	0.469	-0.481	0.348	-0.254	+34	+89
15C	0.516	-0.661	0.758	-0.459	-31	+44

peak tensile stresses (P1) occurred in the superior cortex of the femoral neck, while the maximum compressive stresses (P3) occurred within the medial calcar region. The stress state for the loading condition representing a fall was very different for Femur B, where the maximum tensile and compressive stresses both occurred in the proximal intertrochanteric region on the anterior and posterior sides, respectively. When the results of both models were scaled such that the applied loads were of equivalent magnitude, the peak cervical stresses at impact of a fall in Femur B were 2.6 (P1) and 1.3 (P3) times greater than those calculated for one-legged stance in Femur A. The direction of these principal stress vectors for Femur B demonstrate that, while the femoral neck was primarily in bending, the diaphysis was in torsion.

The predicted von Mises effective stress within the metaphyseal shell was also calculated to evaluate the general distribution of stress. For Femur A (one-legged stance), the peak

Table 5 Results: linear FEA and in vitro bone studies

Model	Analysis	Failure criteria	Experiment (N)	FEA (N)	Percent difference	
A	Yield	Linear	vM Stress	1957	870	-56
			Hoffman		1550	-21
Fracture	Linear	vM Stress	3825	3130	-18	
				vM Strain	2400	+22
Fracture	Linear	vM Strain		3530	-8	
B	Yield	Linear	vM Stress	778	360	-54
			Hoffman		1100	+41
Fracture	Linear	vM Stress	1430	1710	+20	
				vM Strain	740	-4
Fracture	Linear	vM Strain		1360	-5	

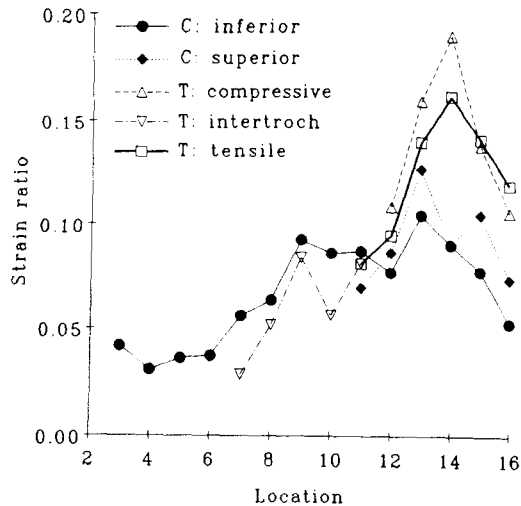


Fig. 6 Maximum ratio between the von Mises strain and the estimated ultimate strain at each section predicted for Femur A (one-legged stance). The filled symbols indicate cortical bone.

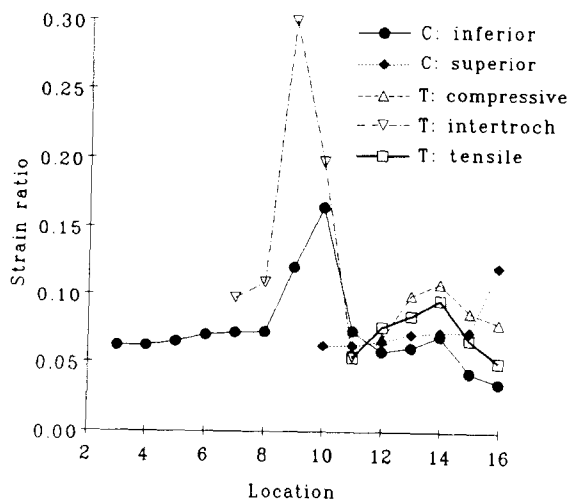


Fig. 7 Maximum ratio between the von Mises strain and the estimated ultimate strain at each section predicted for Femur B (fall). The filled symbols indicate cortical bone.

von Mises effective stresses occur within the superior and inferior bone throughout the femoral neck. In contrast, for Femur B (fall), the peak von Mises effective stresses occur on the anterior and posterior surfaces. However, within the cervical region of both models, the trabecular bone von Mises effective stresses were consistently highest within the elements representing the primary compressive system of trabeculae.

The ratio between the calculated von Mises stress and the model estimated failure stress was calculated separately for cortical bone, the primary compressive trabeculae, and the primary tensile trabeculae. This ratio reaches unity when the von Mises effective stress becomes equal to the bone strength

and hence local failure is expected. For Femur A, the peak cortical stress ratio occurred at the inferior surface at base of the neck (Section 11), while for Femur B, this peak cortical stress ratio occurred at the posterior intertrochanteric region (section 10). In both models, the cortical stress ratio decreased gradually in both the proximal and distal directions. By linear extrapolation cortical failure for Femur A was expected at 3200 N, or 16 percent below the observed in vitro failure load (Table 5). Similarly for Femur B, cortical bone failure was expected at 1600 N, or 12 percent higher than that observed in vitro.

For Femur A, the peak trabecular stress ratio (von Mises/Model predicted) is in the primary compressive trabeculae at section 14. This value, 0.5, suggest that trabecular failure begins much earlier than cortical bone failure, becoming unity at 870 N. In contrast, while a local peak trabecular stress ratio occurs at the same cervical location for Model B (section 14), the maximum value is reached within the intertrochanteric region.

Plots of the peak von Mises strain ratios are presented in Figs. 6 and 7, for Femurs A and B, respectively. For Femur A, the cortical bone trends were somewhat different than those observed for the stress data. The peak strain value occurred on the superior aspect of the femoral neck at section 13. This strain ratio (0.13) reaches 1 at 3530 N which is within 8 percent of the in vitro fracture load. In contrast, the trends of the strain ratios for the trabecular bone were similar to those of the stress ratios with the peak value also occurring at Section 14 (0.18). This value reaches unity at 2400 N, which is 22 percent higher than the load at which the experimental data suggest the intact bone began to behave nonlinearly (1960 N).

For Femur B, the trends in the peak strain ratios were similar to those of the stress ratio data for both cortical and trabecular bone. The peak cortical strain ratio was 0.17 and occurred within the posterior cortex at section 10. This ratio can be extrapolated to an expected failure load of 1360 N, or 5 percent lower than that measured in vitro. The peak trabecular strain ratio was 0.30 and occurred within the intertrochanteric region at section 9. This ratio becomes unity at 740 N, which is 4 percent lower than the load at which the experimental data demonstrated that the intact bone began to behave nonlinearly (778 N).

Discussion

This study demonstrates that the finite element method of analysis, with geometries and material properties generated by the noninvasive imaging technique quantitative computed tomography, can provide an excellent method for estimating the strength of the proximal femur. The results of our analyses compared well with the observed in vitro yield and ultimate bone behavior, however, the predicted surface stresses correlated poorly with direct strain gage measurements. The calculated von Mises effective strain provided the best indicator of both bone yield and failure, predicting bone failure to within 8 percent of the experimental fracture loads measured for both load cases. The onset of structural yielding was observed to result from the initiation of trabecular failure and was also predicted with good accuracy by using the strain failure criteria.

In contrast to the results of the yield and failure studies, our strain gage data correlated poorly with the results of the linear, anisotropic finite element model. Comparisons between strain gage and finite element data has been presented by several authors, the results of which can be used to determine the degree of agreement generally expected. Huiskes et al. [16] conducted an in-depth strain gage study of the femoral diaphysis and reported agreement between beam theory and strain gage data of better than 50 percent when the principal elastic modulus was assumed to be 20 GPa. Similarly, Rohlmann et al. [36] compared the results of detailed finite element studies

of the femur with strain gage data collected from the contralateral bone. The finite element model was typically stiffer than the experimental bone, with reported principal strains of up to 40 percent less than the corresponding measured strains. In general, both studies demonstrated best correspondence in the mid-diaphysis, away from the metaphyseal regions. In contrast, significant discrepancies existed between our FEA predictions and the strain gage data. The finite element model generally predicted larger strains than were measured experimentally. One possible explanation for these large errors was poor gage adherence due to the irregular bone surface conditions present. In contrast to the diaphyseal region, the proximal femur contains an irregular, thin cortical shell with many defects present to allow penetration of nutrient arteries. It proved difficult to find locations where a uniform, flat surface of sufficient area for the entire gage could be provided.

The structural importance of the Ward's triangle region has been stressed by several authors [44], primarily in regard to the use of noninvasive techniques for fracture risk assessment [26]. While the interest in Ward's triangle originated from observations that it is the area in which bone loss appears first [17], this observation alone does not prove structural significance. In fact, the finding that bone in this region is lost first may well indicate its lack of structural importance. Accordingly, the results of our structural analysis demonstrate that this region (sections 11 and 12 for both models) is relatively unimportant in regard to both cortical and trabecular bone stresses and strains. The dramatic loss in density observed in the Ward's triangle region is likely just the consequence of this region having an initially reduced bone density relative to surrounding tissue. A similar process has been noted in the spine, where the nature of the initial trabecular architecture results in the false appearance of preferential bone loss with the progression of osteoporosis [39]. This being the case, measurements at this site may initially be sensitive to bone status, but once the majority of trabecular bone is lost (resulting in the classic appearance of the Ward's triangle), continued measurements at this location will be rather insensitive to further changes. As demonstrated in Figs. 6 and 7, critical strain regions exist more distally, within the intertrochanteric region during impact of a fall (Femur B), and more proximally, within the subcapital region during one-legged stance (Femur A). Consequently, it is likely that Ward's triangle will not be the most sensitive location to make noninvasive bone measurements for the assessment of fracture risk. Rather, to the extent that our simplified loading represents that present in vivo, the intertrochanteric region would appear to be the more sensitive site to assess fall fracture risk, as would the subcapital region for one-legged stance. However, these stress sensitive sites may change provided different or more complete representations of the loading on the proximal femur were used (e.g., the inclusion of a trochanteric load for one-legged stance).

While the loading conditions modeled in this study were not meant to accurately represent those present in vivo, the primary significance of this research is that finite element analysis can be used to accurately predict bone failure provided the loads are accurately known. Therefore, before in vivo fracture risk can be accurately assessed using finite element analysis, the nature of the loads present during actual trauma remain to be determined. However, computed tomography generated finite element analysis may not be the most efficient technique for clinical fracture risk assessment. At present only the determination of trabecular bone material properties is performed in any automated fashion, and generating a well behaved mesh geometry from the computed tomography images is still a process which requires much user interaction. Rather, finite element analysis will likely be of most value for gaining understanding of the processes that occur during bone failure. In addition such analyses may well help optimize attempts to assess bone strength in vivo. Accordingly, the goal of our

additional studies presented elsewhere [23] was to make use of the results of this investigation and to determine the computed tomography based parameters that best relate to the fracture load of intact femoral specimens tested to failure in vitro under the 'fall' loading conditions presented in this study.

There are several potential limitations to this present study. First is the use of isotropic material properties for trabecular bone. While the trabecular bone within the femoral neck and intertrochanteric regions has been shown to demonstrate significant anisotropic behavior [6, 24, 39], Brown et al. [5] demonstrated that the incorporation of anisotropic properties into two-dimensional models of the proximal femur results in no significant changes in the stress distributions. However, these two-dimensional analyses presented by Brown et al. were performed only for simulated one-legged stance in which the applied loads closely align with the principal material directions. During a fall this is not the case and hence such insensitivity to anisotropy may not be apparent. Therefore, the importance of the assumption of isotropy should be investigated.

A second limitation was the simplicity of the load cases considered. The one-legged stance condition neglected muscular loading at the greater trochanter. Consequently differences may exist in the stress within the intertrochanteric region between the state modeled here and that present in vivo during one-legged stance. Given the current understanding regarding loads present during gait, a refined analysis using a more accurate representation of the loading should be performed before the mechanics of spontaneous hip fracture are completely understood.

Fewer quantitative data exist regarding the nature of the applied forces resulting from a fall. Several clinical studies have been performed to attempt to elucidate the most common type of trauma resulting in hip fracture. In an investigation of 365 intracapsular fracture patients, Linton [19] reported that the majority (70 percent) stated that the fracture was caused by a "blow on the hip." Similar results were reported by Backman [3] who stated that 84 of 102 fracture patients recounted a fall on the hip as the cause of fracture. In addition, several experimental studies have been performed with the goal of identifying the intrinsic (muscular) and extrinsic (applied) forces required to produce clinically significant fracture types [40, 38, 3]. Yet, no quantitative data exist regarding the magnitude and direction of forces, both intrinsic and extrinsic, present during falls. The complexity of the problem is compounded by the number of variables which exist, such as patient height and weight, presence of overlying soft tissue, direction of fall, and location of impact. The simplified fall considered here demonstrates that significantly different failure modes can exist for different loading conditions. However, more data regarding the magnitude and direction of the loads present during trauma are needed before the nature of in vivo hip fracture can be completely understood.

A third limitation of the present study is that only linear material properties were considered. Trabecular bone exhibits significant nonlinear behavior and hence regions of bone consisting of significant portions of trabecular bone may be more accurately modeled using nonlinear methods [27]. A more accurate representation was employed in the companion paper [20], to add insight to the events occurring near the time of failure.

A fourth limitation is the use of failure criteria which are open in the triaxial compression direction of principal stress space. This limitation will cause the overestimation of the strength of those elements under significant hydrostatic compression. However, upon review of the stress predictions of our finite element models, the hydrostatic component of the state of stress was small and hence the accuracy of these failure criteria should not be significantly affected.

In summary, the finite element method of analysis was shown to accurately predict both structural yielding and catastrophic

failure for two disparate loading conditions. For a simplified one-legged stance configuration, the primary compressive trabeculae of the subcapital region was the site at which peak stresses occurred. In contrast, during a simplified fall (meant to represent the situation when a patient lands on the lateral buttock/greater trochanter), peak stresses occur in the intertrochanteric region. These results suggest that the intertrochanteric region may be the most sensitive site at which to make noninvasive measurements for the assessment of in vivo fall fracture risk.

Acknowledgments

This study was supported by grants from the National Institutes of Health (CA 41295), from the National Cancer Institute (CA 40211), and from the Centers for Disease Control (CR 102550) and by the Maurice E. Mueller Professorship of Biomechanics at the Harvard Medical School (WCH). We thank Jeanine Goodwin for assistance in manuscript preparation.

References

- Aitken, J. M., "Relevance of Osteoporosis in Women with Fractures of the Femoral Neck," *Br. Med. J.*, Vol. 288, 1984, pp. 597-601.
- Anonymous, "National Center for Health Statistics. Advance Data from Vital and Health Statistics: 1985 Summary: National Hospital Discharge Survey," Hyattsville, MD, PHS 86-1250, 1986.
- Backman, S., "The Proximal End of the Femur," *Acta Radiol. [Suppl.]*, Vol. 146, 1957.
- Bohr, H., and Schaadt, O., "Bone Mineral Content of Femoral Bone and the Lumbar Spine Measured in Women with Fracture of the Femoral Neck by Dual Photon Absorptiometry," *Clin. Orthop.*, Vol. 179, 1983, pp. 240-245.
- Brown, T. D., and DiGirola, A. M., "A Contact-Coupled Finite Element Analysis of the Natural Adult Hip," *J. Biomech.*, Vol. 17, 1984, pp. 437-448.
- Brown, T. D., and Ferguson, A. B., "Mechanical Property Distributions in the Cancellous Bone of the Human Proximal Femur," *Acta Orthop. Scand.*, Vol. 51, 1980, pp. 429-437.
- Burstein, A. H., Reilly, D. T., and Martens, M., "Aging of Bone Tissue: Mechanical Properties," *J. Bone Joint Surg. [Am]*, Vol. 58, 1976, pp. 82-86.
- Carter, D. R., Schwab, G. H., and Spangler, D. M., "Tensile Fracture of Cancellous Bone," *Acta Orthop. Scand.*, Vol. 51, 1980, pp. 733-741.
- Dalen, N., Hellstrom, L. G., and Jacobson, B., "Bone Mineral Content and Mechanical Strength of the Femoral Neck," *Acta Orthop. Scand.*, Vol. 47, 1976, pp. 503-508.
- Elsasser, U., and Reeve, J., "Bone Density Measurement with Computed Tomography," *Br. Med. Bull.*, Vol. 36, 1980, pp. 293-296.
- Eriksson, S. A. V., and Widhe, T. L., "Bone Mass in Women with Hip Fracture," *Acta Orthop. Scand.*, Vol. 59(1), 1988, pp. 19-23.
- Genant, H. K., and Cann, C. E., "Clinical Impact of Quantitative Computed Tomography for Vertebral Mineral Assessment," *Diagnostic Radiology, 26th Annual Postgraduate Course*, Margulis, A. R., and Gooding, C. A., eds., Univ. California Printing Office, Berkeley, CA, 1983, pp. 445-458.
- Genant, H. K., Ettinger, B., Cann, C. E., Reiser, U., Gordon, G. S., and Kolb, F. O., "Osteoporosis: Assessment by Quantitative Tomography," *Orthop. Clin. North Am.*, Vol. 16(3), 1985, pp. 557-568.
- Hipp, J. A., McBroom, R. J., Cheal, E. J., and Hayes, W. C., "Structural Consequences of Endosteal Metastatic Lesions in Long Bones," *J. Orthop. Res.*, Vol. 7, 1989, pp. 828-837.
- Hoffman, O., "The Brittle Strength of Orthotropic Materials," *J. Composite Mat.*, Vol. 1, 1967, pp. 200-207.
- Huiskes, R., Janssen, J. D., and Slooff, T. J., "A Detailed Comparison of Experimental and Theoretical Stress Analyses of a Human Femur," *Mechanical Properties of Bone*, S. Cowin, ed., Am. Soc. of Mech. Eng., New York, Vol. 45, 1981, pp. 211-234.
- Kerr, R., Resnick, D., Sartoris, D. J., Kursunoglu, S., Pineda, C., Haghghi, P., Greenway, G., and Guerra, J., "Computed Tomography of Proximal Femoral Trabecular Patterns," *J. Orthop. Res.*, Vol. 4, 1986, pp. 45-56.
- Leichter, I., Margulies, J. Y., Weinreb, A., Mizrahi, J., Robin, G. C., Conforty, B., Makin, M., and Bloch, B., "The Relationship Between Bone Density, Mineral Content, and Mechanical Strength in the Femoral Neck," *Clin. Orthop.*, Vol. 163, 1982, pp. 272-281.
- Linton, P., "On the Different Types of Intracapsular Fractures of the Femoral Neck," *Acta Chir. Scand. [Suppl.]*, Vol. 86, 1944, pp. 1-118.
- Lotz, J. C., Cheal, E. J., and Hayes, W. C., "Fracture Prediction for the Proximal Femur using Finite Element Models Based on Quantitative Computed Tomography: Part II—Nonlinear Analysis," *ASME JOURNAL OF BIOMECHANICAL ENGINEERING*, published in this issue pp. 361-365.
- Lotz, J. C., Gerhart, T. N., and Hayes, W. C., "Mechanical Properties of Metaphyseal Bone in the Proximal Femur," *J. Biomech.*, Vol. 24, 1991, pp. 317-329.
- Lotz, J. C., Gerhart, T. N., and Hayes, W. C., "Mechanical Properties of Trabecular Bone from the Proximal Femur by Single-Energy Quantitative Computed Tomography," *J. Comput. Assist. Tomogr.*, Vol. 14, 1990, pp. 107-114.
- Lotz, J. C., and Hayes, W. C., "Estimates of Hip Fracture Risk from Falls using Quantitative Computed Tomography," *J. Bone Joint Surg. [Am]*, Vol. 72, 1990, pp. 689-700.
- Martens, M., Audekercke, R., van Delpert, P., De Meester, P., and Mulier, J. C., "The Mechanical Characteristics of Cancellous Bone at the Upper Femoral Region," *J. Biomech.*, Vol. 16, 1983, pp. 971-983.
- Mazess, R. B., Barden, H., Ettinger, B., and Schultz, E., "Bone Density of the Radius, Spine and Proximal Femur in Osteoporosis," *J. Bone Min. Res.*, Vol. 3, 1988, pp. 13-18.
- Mazess, R. B., and Wahner, H. M., "Nuclear Medicine and Densitometry," *Osteoporosis: Etiology, Diagnosis, and Management*, B. L. Riggs and L. J. Melton, eds., Raven Press, New York, 1988, pp. 251-295.
- McBroom, R. J., Cheal, E. J., and Hayes, W. C., "Strength Reductions from Metastatic Cortical Defects in Long Bones," *J. Orthop. Res.*, Vol. 6, 1988, pp. 369-378.
- Melton, L. J. III, and Riggs, B. L., "Epidemiology of Age-Related Fractures," *The Osteoporotic Syndrome: Detection, Prevention, and Treatment*, L. V. Avioli, ed., Grune & Stratton, Inc., Orlando, 2nd Ed, 1987, pp. 1-30.
- Mizrahi, J., Margulies, J. Y., Leichter, I., and Deutsch, D., "Fracture of the Human Femoral Neck: Effect of Density of the Cancellous Core," *J. Biomed. Eng.*, Vol. 6(1), 1984, pp. 56-62.
- Orr, T. E., Beaupre, G. S., Fhyrie, D. P., Shurman, D. J., and Carter, D. R., "Applications of a Bone Remodeling Theory to Femoral and Tibial Prosthetic Components," *Trans. 34th O.R.S.*, 1988, pp. 100.
- Paganini-Hill, A., Ross, R. K., Gerkins, V. R., Henderson, B. E., Arthur, M., and Mack, T. M., "Menopausal Estrogen Therapy and Hip Fracture," *Ann. Intern. Med.*, Vol. 95, 1981, pp. 28-31.
- Phillips, J. R., Williams, J. F., and Melick, R. A., "Prediction of the Strength of the Neck of Femur from its Radiological Appearance," *Biomed. Eng.*, 1975, pp. 367-372.
- Reilly, D. T., and Burstein, A. H., "The Elastic and Ultimate Properties of Compact Bone Tissue," *J. Biomech.*, Vol. 8, 1975, pp. 393-405.
- Revak, C. S., "Mineral Content of Cortical Bone Measured by Computed Tomography," *J. Comput. Assist. Tomogr.*, Vol. 4-3, 1980, pp. 342-350.
- Rohlmann, A., Mossner, U., Bergman, G., and Kolbel, R., "Finite Element Analysis and Experimental Investigation in a Femur with Hip Endoprosthesis," *J. Biomech.*, Vol. 16, 1983, pp. 727-742.
- Rohlmann, A., Mossner, U., Bergmann, G., and Kolbel, R., "Finite Element Analysis and Experimental Investigation of Stresses in a Femur," *J. Biomed. Eng.*, Vol. 4, 1982, pp. 241-246.
- Sartoris, D. J., Sommer, F. G., Marcus, R., and Madvig, P., "Bone Mineral Density in the Femoral Neck: Quantitative Assessment Using Dual-Energy Projection Radiography," *Am. J. Roentgen.*, Vol. 144, 1985, pp. 605-611.
- Smith, L., "Hip Fracture: The Role of Muscle Contraction or Intrinsic Forces in the Causation of Fractures of the Femoral Neck," *J. Bone Joint Surg. [Am]*, Vol. 35, 1953, pp. 367-382.
- Snyder, B., Edwards, W. T., and Hayes, W. C., "Letter to the Editor: Trabecular Changes with Vertebral Osteoporosis," *N. Engl. J. Med.*, Vol. 319, 1988, pp. 793-794.
- Spears, G. N., and Owen, J. T., "The Etiology of Trochanteric Fractures of the Femur," *J. Bone Joint Surg. [Am]*, Vol. 31, 1949, pp. 548-552.
- Stone, J. L., Beaupre, G. S., and Hayes, W. C., "Multiaxial Strength Characteristics of Trabecular Bone," *J. Biomech.*, Vol. 16, 1983, pp. 743-752.
- Vahey, J. W., and Lewis, J. L., "Elastic Moduli, Yield Stress, and Ultimate Stress of Cancellous Bone in the Canine Proximal Femur," *J. Biomech.*, Vol. 20(1), 1987, pp. 29-33.
- Vichnin, H. H., and Batterman, S. C., "Stress Analysis and Failure Prediction in the Proximal Femur Before and After Total Hip Replacement," *ASME JOURNAL OF BIOMECHANICAL ENGINEERING*, Vol. 108, 1986, pp. 33-41.
- Vose, G. P., and Mack, P. B., "Roentgenologic Assessment of Femoral Neck Density as Related to Fracturing," *Roentgenol.*, Vol. 89, 1963, pp. 1296-1301.
- Wicks, M., Garrett, R., Vernon-Roberts, B., and Fazzalari, N., "Absence of Metabolic Bone Disease in the Proximal Femur in Patients with Fracture of the Femoral Neck," *J. Bone Joint Surg. [Br]*, Vol. 64, 1982, pp. 319-322.